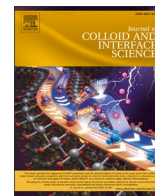




Contents lists available at ScienceDirect

Journal of Colloid And Interface Science

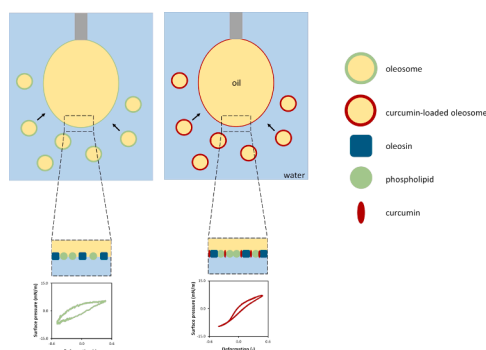
journal homepage: www.elsevier.com/locate/jcis

Regular Article

Modifying the interfacial dynamics of oleosome (lipid droplet) membrane using curcumin

Umay Sevgi Vardar^a, Gijs Konings^a, Jack Yang^{a,b}, Leonard M.C. Sagis^b, Johannes H. Bitter^a, Constantinos V. Nikiforidis^{a,*}^a Laboratory of Biobased Chemistry and Technology, Wageningen University and Research, Bornse Weilanden 9, 6708 WG Wageningen, The Netherlands^b Laboratory of Physics and Physical Chemistry of Foods, Wageningen University and Research, Bornse Weilanden 9, 6708 WG Wageningen, The Netherlands

GRAPHICAL ABSTRACT



ARTICLE INFO

Keywords:
 Natural carrier
 Lipid droplets
 Oil bodies
 Curcumin
 Interfacial rheology

ABSTRACT

Cells store energy in lipid droplets, known as oleosomes, which have a neutral lipid core surrounded by a dilatible membrane of phospholipids and proteins. Oleosomes can be loaded with therapeutic lipophilic cargos through their permeable membrane and used as carriers. However, the cargo can also adsorb between the phospholipids and affect the membrane properties. In the present work, we investigated the effect of adsorbed curcumin on the mechanical properties of oleosome membranes using dilatational interfacial rheology (LAOD). The oleosome membrane had a weak-stretchable behavior, while the adsorption of curcumin led to stronger in-plane interactions, which were dependent on curcumin concentration and indicated a glassy-like structure. Our findings showed that adsorbed curcumin molecules can enhance the molecular interactions on the oleosome membrane. This behavior suggests that oleosomes membranes can be modulated by loaded cargo. Understanding cargo and membrane interactions can help to design oleosome-based formulations with tailored mechanical properties for applications.

* Corresponding author.

E-mail address: costas.nikiforidis@wur.nl (C.V. Nikiforidis).<https://doi.org/10.1016/j.jcis.2024.09.181>

Received 25 March 2024; Received in revised form 9 September 2024; Accepted 21 September 2024

Available online 23 September 2024

0021-9797/© 2024 The Authors. Published by Elsevier Inc. This is an open access article under the CC BY license (<http://creativecommons.org/licenses/by/4.0/>).

1. Introduction

The utilization of synthetic lipid-based carriers such as emulsion, micelle, and liposome is the most frequently employed strategy to improve lipophilic therapeutic delivery efficiency [1,2]. Although the lipid-based carriers successfully enhance poor bioavailability, low water solubility, and low stability of lipophilic therapeutics [3]. Due to sustainability and health concerns about the proposed carriers, the demand for green-natural carrier/delivery systems has recently increased. To meet the demands of society, oleosomes can be adapted as natural carriers [4–6].

Oleosomes are specialized organelles that store energy and carry fat-soluble vitamins and other lipophilic molecules in eukaryotic cells [7]. Oleosomes naturally occur in plant seeds as ready-to-use lipid shuttles, having a triacylglycerol core surrounded by a phospholipid-protein monolayer membrane, which stabilizes the oleosomes against lipid oxidation [8]. The stabilization is attributed to the interaction between phospholipids and oleosin through hydrophobic and electrostatic forces. In the membrane, phosphatidylcholine and phosphatidylserine are the most abundant phospholipids, whereas oleosins are the main membrane proteins [7,8]. In addition to protecting oleosomes against coalescence, the oleosome membrane is selectively permeable for lipophilic molecules, and this behavior allows the loading and carrying of lipophilic molecules [4,6,9].

As previously shown, curcumin is a lipophilic molecule with potential therapeutic properties that can spontaneously diffuse into the oleosome core [6,10]. It has been shown that curcumin is not exclusively located in the core of oleosomes, but is also adsorbed at the oleosome membrane [6]. The localization of curcumin at the oleosome membrane can impact oleosome stability and efficiency. Therefore, the interaction between the oleosomes membrane and loaded molecules must be well-defined in order to design oleosomes as lipid carriers for lipophilic molecules.

The impact of curcumin molecules on the oleosome membrane can be studied by interfacial rheology, which gives insight into how curcumin affects the mechanical properties of the oleosome membrane. A few studies have already explored the mechanical properties of oleosome membranes, specifically focusing on the interaction of membrane proteins and phospholipids using interfacial rheology [11–16]. These studies primarily investigated oleosome behavior at oil/water or air/water interfaces. For instance, it has been shown that the intact oleosomes can absorb into an air–water interface. This adsorption is then followed by the rupture and spreading of the phospholipids and membrane proteins over the air–water interface [12,15]. Further, spreading materials at the interface leads to the formation of an interfacial film, and the application of forces causes the deformation of the film, which helps estimate the mechanical properties of the oleosome membrane. Oleosomes formed a stretchable film at the air–water interface; similarly, it was found that the interfacial stabilization of oleosomes is highly related to their membrane fragments at oil–water [11,12].

In addition to the oleosome membrane, the curcumin impact on the phospholipid membrane highly depends on the lipid composition of the membrane. Karewicz et al. showed that curcumin had a condensing effect on egg yolk phosphatidylcholine (EYPC) and EYPC/dihexadecyl phosphate (DHP) monolayer membranes. Here, curcumin showed a similar effect to cholesterol on the monolayer membrane. However, in the case of the EYPC/DHP/cholesterol monolayer membrane, since cholesterol has already shown a strong ordering effect on the monolayer membrane, adding curcumin disturbs this arrangement and causes loosening on the monolayer [17]. Sun et al. highlighted that curcumin binding decreased the thickness of the lipid layers and reduced their rigidity. More specifically, the addition of curcumin altered the physical properties of the lipid layers by causing an interfacial area expansion [18]. However, these studies focused on only phospholipid membrane and curcumin interactions. The effect of loaded curcumin on the oleosome's phospholipid-protein membrane interfacial properties is still

unclear.

Therefore, in this study, our aim was to understand whether curcumin influences the mechanical properties of the oleosome membrane and the molecular-level interactions between the membrane molecules using surface dilatational rheology. Understanding the interactions of lipophilic cargoes with the oleosome membrane gives further insights into the potential of tailoring the mechanical properties of the oleosome membrane and achieving a targeted delivery.

2. Materials and methods

2.1. Materials

Oleosomes were extracted from untreated Alizze rapeseeds. Rapeseed oil was purchased from a local market, and curcumin (95 % purity) was purchased from Alfa Aesar (UK). All other chemicals were of analytical grade and were purchased from Sigma Aldrich (St Louis, MO, USA). All solutions were prepared with ultrapure water.

2.2. Methods

2.2.1. Oleosome extraction

Oleosomes were extracted based on the procedure described in previous work [19]. Rapeseeds were dispersed in 0.1 M NaHCO₃ (pH 9.5) and kept at room temperature for 4 h under continuous magnetic stirring (VMS-C7 WVR Advanced). The rapeseed-NaHCO₃ dispersion was subsequently blended for 1 min at maximum speed with a blender (Waring 8010ES blender), and then the slurry was filtered by using a cheesecloth (GEFU®, Eslohe, Germany). The obtained filtrate was centrifuged at 10,000g for 30 min at 4 °C (Sorvall Legend XFR, ThermoFisher Scientific, Waltham, MA, USA). After centrifugation, the oleosome cream layer was collected. The cream was further purified by dispersing and centrifuging twice with 0.1 M NaHCO₃ and MilliQ, respectively. After the last centrifugation step, the cream layer was collected and stored in the refrigerator (4 °C).

2.2.2. Composition analysis and electrophoresis

The moisture, oil, and protein content of the oleosome were determined. Moisture content was calculated based on dried matter. The oleosome cream was dried at 60 °C in an oven (Memmert, Memmert GmbH & Co.KG, Schwabach, Germany) until the weight remained constant. Soxhlet extraction was used to determine the oil content of the cream by extraction with petroleum ether, and the extraction was performed for 8 h. The oil content after extraction was calculated by using Eq. (1):

$$\text{oil content (wt\%)} = 100 \times \frac{\text{g of extracted oil}}{\text{g of initial sample}} \quad (1)$$

The protein content of the cream was determined using the Dumas method (Rapid N exceed – N/Protein Analyzer) based on dry matter. A nitrogen conversion factor of 5.7 was used. All samples were measured in duplicate.

The protein profile of the oleosome was determined with SDS-PAGE under reducing and non-reducing conditions. Oleosome (13–14 mg) was mixed with 250 μ L sample buffer (NuPAGE LDS, Thermo-Fischer, Landsmeer, the Netherlands), 100 μ L reducing agent (NuPAGE Sample Reducing Agent, ThermoFisher, Landsmeer, the Netherlands) and 650 μ L MilliQ water (reducing conditions), or 250 μ L sample buffer and 750 μ L MilliQ water (non-reducing conditions). The samples were centrifuged for 1 min at 2000 rpm (Sorvall Legend XFR, ThermoFisher Scientific, Waltham, MA, USA). The samples were then heated in an Eppendorf Thermomixer C for 10 min at 70 °C, after which the tubes were centrifuged again. Then, 10 μ L of protein marker (PageRuler Prestained Protein Ladder, 10–180 kDa, ThermoFisher, Landsmeer, the Netherlands) and 18 μ L of the sample were loaded onto the gel (NuPAGE Novex 4–12 % Bis-Tris Gel, ThermoFisher, Landsmeer, the Netherlands).

MES was used as a running buffer (NuPAGE MES SDS Running Buffer, ThermoFisher, Landsmeer, the Netherlands). The gel was run for approximately 30 min at 200 V and 160 mA. The gel was washed three times with MilliQ water and stained (Coomassie Brilliant Blue R-250 Staining Solution, Bio-Rad Laboratories B.V., Lunteren, the Netherlands) for one hour under gentle shaking. Subsequent de-staining was done with a solution of 10 % ethanol and 7.5 % acetic acid in MilliQ water overnight. Images of the gels were made with a Biorad GS900 Gelscanner and accompanying Image Lab software. All samples were measured in duplicate.

2.2.3. Oleosome emulsion preparation and curcumin encapsulation

Oleosome (10 wt%) was dispersed in MilliQ water at room temperature by stirring for 1 h. The pH-driven method was used to produce curcumin-loaded oleosomes using the method reported by Zheng et al. [4] with some modifications. Along with the modification, a stock alkaline curcumin solution (10 mg/g), was prepared by dissolving curcumin into NaOH solution (0.2 M, pH 12.5) in the dark at ambient temperature for 2 min. A known amount of stock curcumin alkaline solution was mixed with oleosome emulsion, and then the mixture was immediately adjusted to pH 7.0. The final emulsion contained 0.1 and 1 mg curcumin per g oleosome cream. Finally, curcumin-loaded oleosome emulsions were stored in the refrigerator (4 °C) until further analysis.

2.2.4. Encapsulation efficiency

Curcumin-loaded oleosomes were centrifuged for 15 min at 10,000 rpm and 4 °C (Sorvall Legend XFR, ThermoFisher Scientific, Waltham, MA, USA), after which the curcumin-loaded yellow cream was carefully removed from the aqueous phase. The aqueous phase was mixed with ethanol and then vortexed. Free curcumin in the aqueous phase was analyzed by using a UV-spectrophotometer (UV1600 PC Spectrophotometer, VWR) at 424 nm. The encapsulation efficiency was calculated by using Eq. (2):

$$\text{Encapsulation efficiency} = 100 * \left(\frac{C_{\text{initial}} - C_{\text{unencapsulated}}}{C_{\text{initial}}} \right) \quad (2)$$

Here, C_{initial} and $C_{\text{unencapsulated}}$ are the concentrations of curcumin initially added to the system and the concentration of free curcumin [20]. All samples were measured in duplicate.

2.2.5. Microscopy

A confocal laser scanning microscope (CLSM, Leica SP8-SMD microscope, Leica Microsystems, Wetzlar, Germany) was used to visualize the microstructure of the curcumin-loaded oleosome. The microscope was fitted with a 63 × objective-water immersion lens, and an Argon ion laser was used to image the samples. Curcumin was excited at 458 nm, and the emission was captured between 470 and 500 nm. All samples were measured in duplicate.

2.2.6. Particle size distribution

The particle size distribution of the oleosomes was determined by laser diffraction (Better Sizer S3 Plus, China). To investigate the presence of aggregated oleosomes and determine their actual size, 1.0 wt% sodium dodecyl sulphate (SDS) was added to the sample (1:1). The used refractive index was 1.47 for rapeseed oil and 1.333 for water. Measurements are reported as the volume mean diameter:

$$d_{4,3} = \frac{\sum n_i d_i^4}{\sum n_i d_i^3} \quad (3)$$

Here, n_i is the number of droplets with a diameter of d_i . All samples were measured in triplicate.

2.2.7. Interfacial dilatational rheology

The interfacial dilatational rheology was investigated using an automatic drop tensiometer (ADT, Teclis TRACKER, France). A pendant water droplet with a surface area of 30 mm² was created at the tip of a

needle (straight Teflon coated G20/0.60 mm) in a cuvette filled with stripped rapeseed oil. The water phase contained a 1 wt% oleosome solution with 0 %, 0.01 %, or 0.1 % loaded curcumin at pH 7.0. Rapeseed oil was stripped by mixing 2:1 with activated magnesium silicate (Florisil) for 24 h, then centrifuged twice for 20 min at 2000 rpm and 20 °C, separating the supernatant oil each time.

The interfacial tension was monitored for 2 h at 20 °C. During this waiting time, the droplet shape was captured with a camera, and the droplet's contour was fitted using the Young-Laplace equation to calculate the surface stress. After 2 h of waiting time, oscillatory dilatational deformations were applied. A repetition of five oscillations in area, with a frequency of 0.02 Hz, was performed at amplitudes from 5 % to 50 % in an increasing manner. The interface was left for a 15 min to rest between each set of oscillations.

All measurements were measured in duplicate. The surface stress response was used to determine surface dilatational moduli and to construct Lissajous curves. Lissajous curves of the surface pressure ($\Pi = \gamma - \gamma_0$) versus the deformation ($(A - A_0)/A_0$) were plotted from the middle three oscillations of each amplitude cycle. Here, γ and γ_0 are the surface tension of the deformed and non-deformed interface, and A and A_0 are the areas of the deformed and non-deformed interface.

2.2.8. General stress decomposition

A general stress decomposition (GSD) was implemented by utilizing a MATLAB (2020b) script [21]. The middle three oscillations from every five oscillation cycles were extracted and interpolated over a full period. Then, we performed a Fourier transform on the interpolated signal. We did not include the harmonics that have an intensity below 3 % of the first harmonic to the transform as they were noise.

The GSD separates the overall stress in a contribution from the odd harmonics and a contribution from the even harmonics of the Fourier transform, and then further separates these two stresses in an elastic and a viscous contribution. Here, τ_1 represents the elastic and τ_2 the viscous contribution to the odd harmonics: τ_3 represents the viscous contribution and τ_4 the elastic contribution to the even harmonics. Several other features of the interface were calculated by using these stress components ($\tau_1, \tau_2, \tau_3, \tau_4$).

To calculate the modulus at 0 strain ($E_{\tau 1M} = \left. \frac{d\tau_1}{d\varepsilon} \right|_{\varepsilon=0}$), Eq. (4) was used. Here, b'_{2k+1} is the amplitude of the corresponding harmonic extracted from the Fourier series and ε_0 is the strain amplitude.

$$E_{\tau 1M} = \left. \frac{d\tau_1}{d\varepsilon} \right|_{\varepsilon=0} = \frac{\sum_{k=0}^n (2k+1)b'_{2k+1}}{\varepsilon_0} \quad (4)$$

To calculate the strain softening factor (S) of $E_{\tau 1}$, Eq. (5) was used. Here, $E_{\tau 1L} = \left. \frac{\tau_1}{\varepsilon} \right|_{\varepsilon=\pm\varepsilon_0}$ is the stress of τ_1 at maximum strain divided by the strain amplitude.

$$S = \frac{E_{\tau 1L} - E_{\tau 1M}}{E_{\tau 1L}} \quad (5)$$

According to Eq. (6), $E_{\tau 4}$ is the secant modulus of τ_4 was calculated. Here, d_{4k+2} is the amplitude of the relevant harmonics.

$$E_{\tau 4} = - \frac{\sum_{k=0}^n 2d_{4k+2}}{\varepsilon_0} \quad (6)$$

To determine the dissipated energy ($U_{d\tau 2}$) for τ_2 and the total dissipated energy ($U_{d\tau 3}$) for τ_3 , Eqs. (7) and (8) were used [21]. Here, E_1^* is the first harmonic-based loss modulus and $E_{2k\tau 3}$ is the even harmonics-loss modulus of the $2k^{\text{th}}$ mode.

$$U_{d\tau 2} = \pi \varepsilon_0^2 E_1^* \quad (7)$$

$$U_{d\tau 3} = \oint \tau_3(t) \dot{\gamma}(t) dt = 2\varepsilon_0^2 \sum_{k=1}^n \left(\frac{E_{2k\tau 3}^* k}{k^2 - 1/4} \right) \quad (8)$$

Equation (9) was used to calculate the plots' vertical shift, with d_0' is the 0th harmonic of the Fourier transform.

$$\gamma_s = d_0' \quad (9)$$

3. Result and discussion

3.1. Oleosome characterization and curcumin encapsulation

The composition of the obtained rapeseed oleosome extract was determined and found that the moisture content was approximately 29.9 ± 1.2 wt%, the oil content was 68.8 ± 0.6 wt%, and the protein content was 0.9 ± 0.01 wt%. The proteins on oleosomes were also analyzed qualitatively using SDS-PAGE and found only one band at 18 kDa, indicating that predominantly only the oleosome proteins, oleosins, were present [22].

The obtained oleosome extract was also analyzed for the droplet size distribution. The obtained curve showed a narrow size distribution with a monomodal peak, with $d_{4,3}$ was $1.45 \mu\text{m}$ (Fig. S1A).

Following, curcumin at two different concentrations was loaded into oleosomes, and loading was confirmed by CLSM (Fig. S1B and C). Encapsulation efficiency of 0.01 wt% curcumin into 10 wt% oleosomes (COLE-1) was found to be 100 ± 0.00 %. This result also coincides with our previous work [6]. However, we found that the encapsulation efficiency of 0.1 wt% curcumin (COLE-2) was 61.57 ± 0.16 %. Encapsulation at both curcumin concentrations did not show an impact on oleosome particle sizes (Fig. S1A).

3.2. Interfacial properties of oleosomes

The amphiphilic and interfacial-active curcumin molecules adsorb at the o/w interface of oleosomes and interact with the oleosome membrane [6]. Although curcumin's encapsulation did not impact the oleosomes size distribution, the molecular interactions between curcumin and membrane could still affect oleosomes stability. To gain more insights into the effect of curcumin on the oleosome membrane, the interfacial properties of the oleosome membrane were evaluated using a drop tensiometer.

3.2.1. Adsorption behavior

The interfacial tension of the oleosome dispersions was determined as a function of time to investigate the adsorption behavior of oleosomes and curcumin-loaded oleosomes at the oil–water interface. As shown in Fig. 1A, oleosomes immediately decreased the surface tension directly after 1 s and decreased the interfacial tension from 30 mN/m to 19 mN/m in 7200 s. This indicates that sufficient oleosome concentration (1 wt

%) is present in the droplet to decrease surface tension without a lag phase (i.e., an initial phase where surface tension does not decrease).

First, oleosomes diffuse and adsorb at the interface, followed by adsorption, rupture, and spreading of the membrane material [11,15]. The adsorption behavior of molecules can be summarized as diffusion towards the interface, adsorption, and structural rearrangement [23]. During the adsorption phase, oleosomes rapidly adsorbed at the oil–water interface after droplet formation, and the interfacial tension displayed a decline. However, due to their hydrophilic exterior, oleosomes are unlikely to act as surfactants between oil and water. Oleosomes (OLE) must have diffused randomly in the water phase, occasionally approaching the interface within a very small distance [24–26]. In close proximity to the interface, the oleosome could have deformed, followed by rupture of the thin water film between the external oil phase and the oil phase of the oleosome, and as a result, membrane molecules spread onto the interface [12,27].

In the case of curcumin-loaded oleosomes (COLEs), COLE-1 (included 0.01 wt% curcumin) reduced the interfacial tension from 29 mN/m to 19 mN/m, and COLE-2 (included 0.1 wt% curcumin) reduced the interfacial tension from 30 mN/m to 18 mN/m in 7200 s (Fig. 1A). Although the final interfacial tension values of curcumin-loaded oleosomes were not significantly different from oleosomes. Here, different adsorption kinetics were observed in the initial stages. For COLE-1, curcumin and oleosomes showed a mutual effect on kinetics, and COLE-1 acted more surface active than oleosomes. For COLE-2, a similar kinetic pattern was expected; however, COLE-2 showed less surface activity than COLE-1. To understand why COLE-2 showed different behavior than COLE-1, the membrane's mechanical properties must be investigated.

Further, the surface activity of 0.01 wt% curcumin was measured to understand the impact of non-encapsulated curcumin on the interface. The non-encapsulated curcumin decreased the interfacial tension from 30 mN/m to 20 mN/m in 7200 s. Curcumin shows slight surface activity but does not reach the surface tension values of the COLE-1. Based on this, we assume the curcumin is mostly introduced by the rupture of oleosomes at the oil–water interface, especially as 100wt% of the curcumin was encapsulated for the COLE-1. For the COLE-2, lower surface tension was obtained due to higher curcumin concentrations in the oleosome.

3.2.2. Dilatational interfacial rheology

After 2 h of waiting time, an interfacial layer was formed by the oleosomes or curcumin-loaded oleosomes, and interfacial dilatational deformations were applied to understand the impact of curcumin on the mechanical properties of the oleosome membrane. Amplitude sweeps

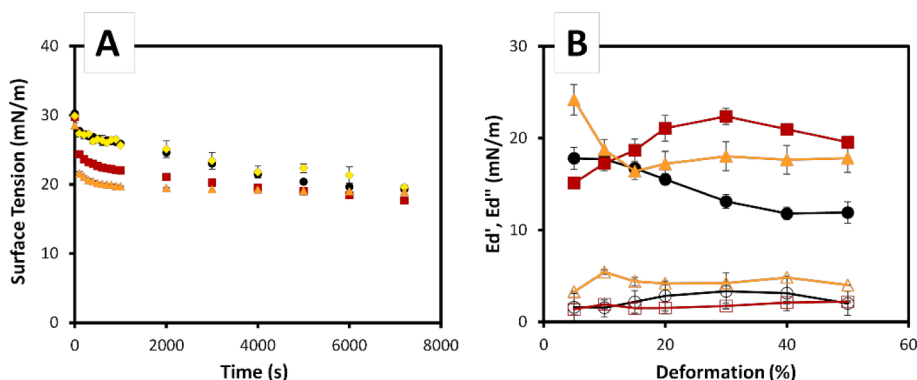


Fig. 1. (A) Dynamic interfacial tension of oleosome (OLE, black \circ), curcumin-loaded oleosome (COLE-1, orange Δ and COLE-2, red \square) emulsions at 1 wt% oleosome concentration (pH 7.0, 20 °C), and curcumin (yellow \diamond , 0.1 wt%) (B) Dilatational elastic modulus (E_d' : filled symbol) and viscous modulus (E_d'' : hollow symbol) over deformation amplitude of OLE (\circ), COLE (Δ) and COLE-2 (\square) at a constant frequency of 0.02 Hz. This figure shows the average and standard deviation of duplicate measurements. Both panels show the average of duplicate measurements, including the standard deviations. (For interpretation of the references to colour in this figure legend, the reader is referred to the web version of this article.)

were performed, where the amplitude of deformation was gradually increased, and the obtained surface dilatational elastic (E_d') and viscous (E_d'') moduli of oleosome and curcumin-loaded oleosome stabilized interfacial films are shown in Fig. 1B.

The pure oleosomes (in the absence of curcumin) showed decreasing moduli from 17 mN/m at 5 % deformation to 11 mN/m at 50 % deformation. These are low moduli values compared to, for instance, dairy proteins with values up to 60 mN/m [28], which are able to form stiff solid-like interfacial layers. So, the oleosomes formed substantially weaker interfacial layers compared to proteins, as previously also observed in [11]. A slight amplitude dependence is present, which could be due to network disruptions or changes in surface density upon expansion and compression.

The COLE-1 showed decreasing moduli from 24 mN/m at 5% deformation to 16 mN/m at 15% deformation, then stayed almost constant. While the COLE-2 had markedly different E_d' values, which increased at higher deformations from 17 mN/m at 5% deformation up to 22 mN/m at 30% deformation. At even higher deformations of 40 and 50%, the moduli started to decline to 19 mN/m. Also, the E_d' of COLE-1 and COLE-2 were higher than OLE at deformations above 15%. In

general, the E_d' was higher compared to the E_d'' modulus in all samples, indicating that OLE and COLEs formed films that behave predominantly elastic in the studied range of deformations. The increase of E_d' for COLE-2 was unexpected, as one usually obtains a constant E_d' for very stretchable interfaces or a decreasing E_d' where the interfacial microstructure is disrupted progressively. If curcumin is present between the phospholipids, we might expect an active role here during compression. Prior to further discussing the potential mechanism, we will first discuss the nonlinear contributions to the stress response.

Nonlinear contributions in the surface stress signal are present when deformations are performed in the nonlinear viscoelastic regime (NLVE), which is the case for our systems. The E_d' values are calculated based on the intensity and phase of the first harmonic of the Fourier spectrum, without considering the nonlinearities quantified by the higher harmonics. These nonlinear contributions can be qualitatively analyzed by plotting the raw signals of the surface pressure as a function of deformation in Lissajous plots. For an extensive explanation, we refer to previously published articles [29,30].

Fig. 2 shows the Lissajous plots of interfacial films stabilized by oleosomes in the absence (OLE) and in the presence of curcumin (COLE-

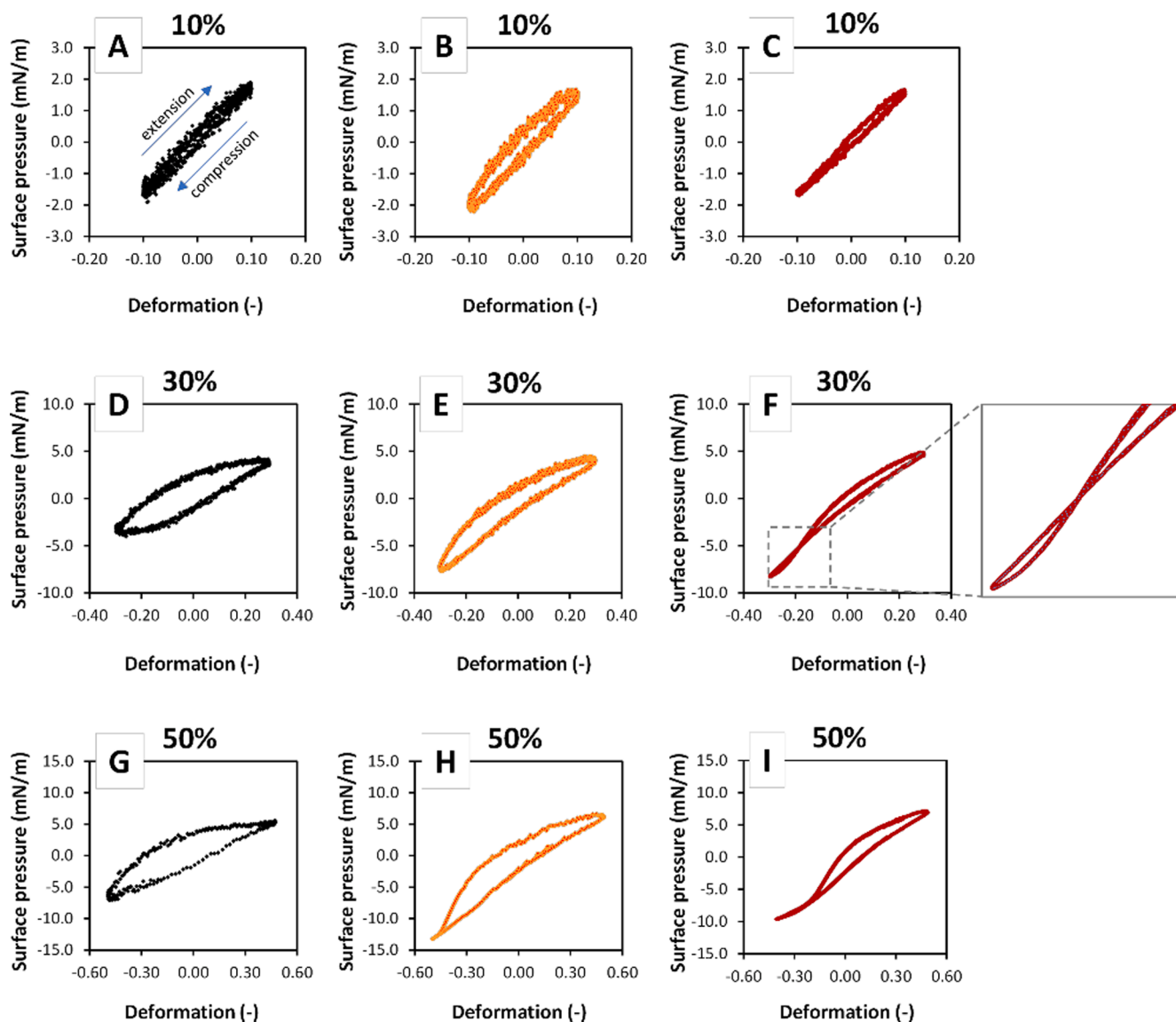


Fig. 2. Lissajous plots of interfacial films stabilized by oleosomes (A, D, G plots, black), 0.01 wt% curcumin-loaded oleosomes (B, E, H plots, orange) and 0.1 wt% curcumin-loaded oleosomes (C, F, I plots, red) at 10, 30 and 50% dilatational deformation and oscillation frequency at 0.02 Hz. (For interpretation of the references to colour in this figure legend, the reader is referred to the web version of this article.)

1 and COLE-2). The Lissajous plots of OLE, COLE-1, and COLE-2 were different at 10, 30, and 50 % amplitude. The Lissajous plots move clockwise, and the loop indicates the cyclic extension and the compression of the interface. The extension takes place in the upper part of the loop, and the compression follows on the bottom side of the loop. The rheological responses are characterized by the width of the loop, where a straight line indicates an elastic response, a circle indicates a viscous response, and an ellipse demonstrates a viscoelastic response.

At 10% amplitude, oleosomes at the interface showed a symmetric narrow loop, suggesting an almost fully elastic response (Fig. 2A). At 30 and 50% amplitude, OLE presented non-linear viscoelastic behavior. At 30% amplitude, the shape of the plot was getting wider and exhibited a slight strain softening in the expansion (Fig. 2D). This is evident from the initially steep increase in surface pressure at the start of expansion (lower left corner), followed by a gradual decrease in the slope of the curve, towards maximum expansion (upper right corner). At 50 % amplitude, the interfacial film showed more significant strain-softening behavior during expansion as the slope of the curve levelled off to near horizontal (Fig. 2G). In the compression cycle (bottom part), the oleosome-stabilized interface started to show a slight strain softening at the end of the compression cycle for 30 % deformation. The strain softening in compression could be the result of the expulsion of the material into the bulk upon compression, indicating weak interactions between the adsorbed interfacial stabilizers.

On the other hand, at 10% amplitude, oleosomes in the presence of curcumin (Fig. 2B, COLE-1, 0.01 wt%) at the interface showed a narrow ellipse shape, which was slightly wider than the plot belonging to OLE (Fig. 2A). At 30 and 50 % amplitude (Fig. 2E–H), the surface pressure reached much more negative values in compression compared to pure OLE films. This means that the interfacial film showed much more extensive strain-hardening behavior during compression. This would already suggest stronger in-plane interactions between adsorbed molecules in the presence of curcumin.

Oleosomes loaded with higher concentrations of curcumin (COLE-2, 0.1 wt%) showed different behavior, particularly at 30 and 50 % amplitude (Fig. 2F–I), at the end of the compression and start of the extension cycle. There is a cross-over at 30 % deformation (see insert) for COLE-2 (Fig. 2F). Such crossovers were previously seen for Lissajous plots of dilatational rheology on saponin escin-stabilized interfaces [31]. The cross-over is the result of a levelling off in the compression cycle. As a result, the leveling off causes the compression cycle to end above the extension cycle, causing a secondary loop. For escin-stabilized interfaces, this behavior was attributed to the formation of very dense layers that start to buckle and form multilayers during compression. These multilayers are then stretched in the extension cycle. This behavior suggested that escin had extremely strong in-plane interaction and formed a stiff glass-like solid layer [31]. As we observe similar (but milder) behavior here for COLE-2, the high concentration of curcumin at the interface might have a similar effect.

It is clear that a highly complex behavior arises when analyzing the Lissajous plots of these interfaces. This response could originate from either network interactions or surface density changes, and these two phenomena cannot be differentiated from the overall Lissajous plots in Fig. 2. Therefore, a recently developed method called the ‘general stress decomposition’ (GSD) was used to separate the two types of contributions [21]. In the GSD, the shape changes can be analyzed in more detail by decomposition of the surface stress into its four basic components τ_1 , τ_2 , τ_3 , and τ_4 , based on the odd and even Fourier harmonics of the surface stress signal. In previous work, the generation of odd harmonics in the surface stress was related to network interactions, while the even harmonics resulted from surface density changes. Both contributions can be further separated into elastic and viscous components. For the odd harmonics, the elastic and viscous components are called τ_1 and τ_2 , respectively, whereas the elastic and viscous contribution of the even harmonics are τ_4 and τ_3 , respectively. The GSD approach was previously used for protein-stabilized interfaces from asparagus [32] and rapeseed.

The four components obtained from the GSD analysis are shown in Fig. 3 for OLE, COLE-1 and COLE-2 at 50 % deformation, which are shown in 4 panels: 1) The full signal ($\tau_1 + \tau_2 + \tau_3 + \tau_4$) is shown in the first row (panel A–C), 2) the combined signals of the odd harmonics ($\tau_1 + \tau_2$) and the elastic component (τ_1) are shown in the second row (panel D–F), 3) the combined signals of the even harmonics ($\tau_3 + \tau_4$) and the elastic component (τ_4) (panel G–I), 4) the individual components of the even harmonics, $\tau_3 + \tau_4$ (panel J–L).

For Fig. 3D–E, a narrow ellipsoidal plot for OLE and COLE-1 in the odd harmonics ($\tau_1 + \tau_2$) was observed, indicating a predominantly elastic behavior without significant network breakdown. COLE-2 (Fig. 3F) has a sigmoidal shape, which in bulk shear rheology is typically associated with softening behavior and could indicate alteration of the interfacial microstructure. In addition, the slopes of the τ_1 around zero strain are higher for this ample, which confirms this sample forms a stiffer interfacial network.

The even harmonics show a large signal for τ_3 and τ_4 , thus indicating a major contribution of the even harmonics to the overall signal (Fig. 3A–C), which is also the main reason for the asymmetric shape of the curve for the total stress. From these plots, we conclude that both network interactions and surface density changes play an important role in all three interfacial films. Conclusions on the three interfaces are difficult to draw, based on the Lissajous plots in Fig. 3 only. Therefore, the plots were further quantified over the whole amplitude sweep with the parameters defined in Eqs. (4) through (9), and the results are shown in Fig. 4.

From the odd harmonics, we obtained the elastic modulus $E_{\tau_{1M}}$ from the slope of τ_1 at zero strain (Fig. 4A), and $U_{d\tau_2}$, the viscous energy dissipation obtained from the area of τ_2 (Fig. 4B). The stiffening factor (S-factor) was obtained from τ_1 and is shown in Fig. 4F. The even harmonics yield the elastic modulus E_{τ_4} by determining the secant modulus of τ_4 at maximum strain (Fig. 4C), the viscous energy dissipation $U_{d\tau_3}$ from the enclosed area of the loop of τ_3 (Fig. 4D), and the vertical shift γ_s (Fig. 4E). The latter is determined from the baseline shift of τ_4 .

The OLE-stabilized interface shows a decrease of the $E_{\tau_{1M}}$ (Fig. 4A) and increasing $U_{d\tau_2}$ (Fig. 4B) upon increasing amplitudes. The decrease of the modulus and increase in energy dissipation is an indication of the structural breakdown of the OLE-stabilized interface. In addition, there is also a strong contribution from the even harmonics, as the E_{τ_4} decreases to more negative values (Fig. 4C) and $U_{d\tau_3}$ increases (Fig. 4D). The GSD analysis shows here for OLE a decrease of network interactions at higher deformation, while surface density changes started to play a more significant role. Such behavior was previously shown for air–water and oil–water interfaces stabilized by oleosomes [11,16], where the interfaces showed structural breakdown first, and then showed a strain softening at the end of the compression cycle at higher deformation. In the OLE sample studied here, the softening in compression is not very evident, as $E_{\tau_{1M}}$ and E_{τ_4} are decreasing smoothly with increasing amplitude.

The COLE-1 showed a different behavior, as $E_{\tau_{1M}}$ (Fig. 4A) was almost constant over the whole deformation range, thus giving higher moduli than OLE at higher strains. In addition, much more negative E_{τ_4} values (Fig. 4C) and a more significant negative shift of γ_s (Fig. 4E) were observed compared to OLE. The higher curcumin content in COLE-2 changed the behavior even more significantly. For COLE-2, the $E_{\tau_{1M}}$ increased from 17 mN/m to 31 mN/m over the whole amplitude range (Fig. 4A), and the $U_{d\tau_2}$ was substantially lower than OLE and COLE-1 (Fig. 4B). An even more interesting behavior is observed in the even harmonics, where the E_{τ_4} of COLE-2 showed a decrease from 0 to -6 mN/m when increasing the deformation from 5 to 30 %, and then it increases back to -1 mN/m when further increasing the deformation to 50 % (Fig. 4C). The COLE-2 also has even lower γ_s than COLE-1 and started to show a very negative S-factor at deformations >30 %, suggesting major strain softening (Fig. 4F).

The higher $E_{\tau_{1M}}$ modulus for COLE-2 suggests stronger network interactions at higher deformations, while the opposite is shown for OLE

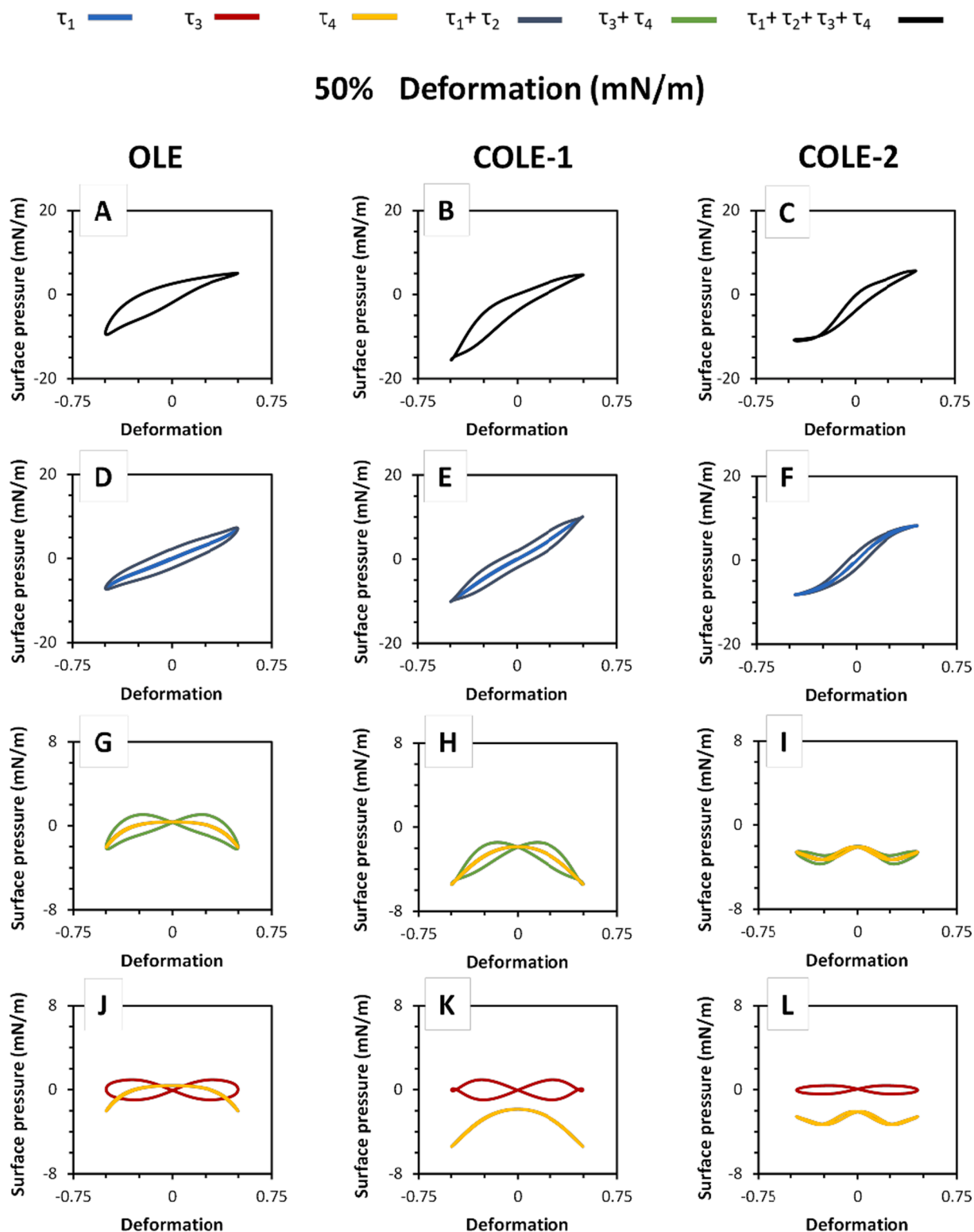


Fig. 3. The decomposed Lissajous plots of oleosomes (OLE), 0.01 and 0.1 wt% curcumin-loaded oleosomes (COLE-1, COLE-2) at oil–water interface at 50 % deformation. A, B, and C plots present the original signals (black). D, E, and F plots show τ_1 (dark blue) and $\tau_1 + \tau_2$ (blue). G, H, and I plots show τ_4 (yellow) and $\tau_3 + \tau_4$ (green). J, K, and L plots show τ_3 (red) and τ_4 (yellow). (For interpretation of the references to colour in this figure legend, the reader is referred to the web version of this article.)

(Fig. 4A). The curcumin seems to induce stronger in-plane interactions within the interfacial microstructure. This, in addition to the substantially lower energy dissipation (U_{dr2} , Fig. 4B) points to the formation of a glassy-like structure, which is also suggested by the flattening off of the overall Lissajous plot and formation of a secondary loop at maximum

compression in the plot of COLE-2 at 30 % deformation. This behavior can be attributed to three phenomena: 1) expulsion of interface stabilizer from the interface into the bulk phase upon compression (and vice versa upon extension), 2) buckling (i.e., out-of-plane deformations) of the interface, or 3) interfacial structures starting to slide over each other,

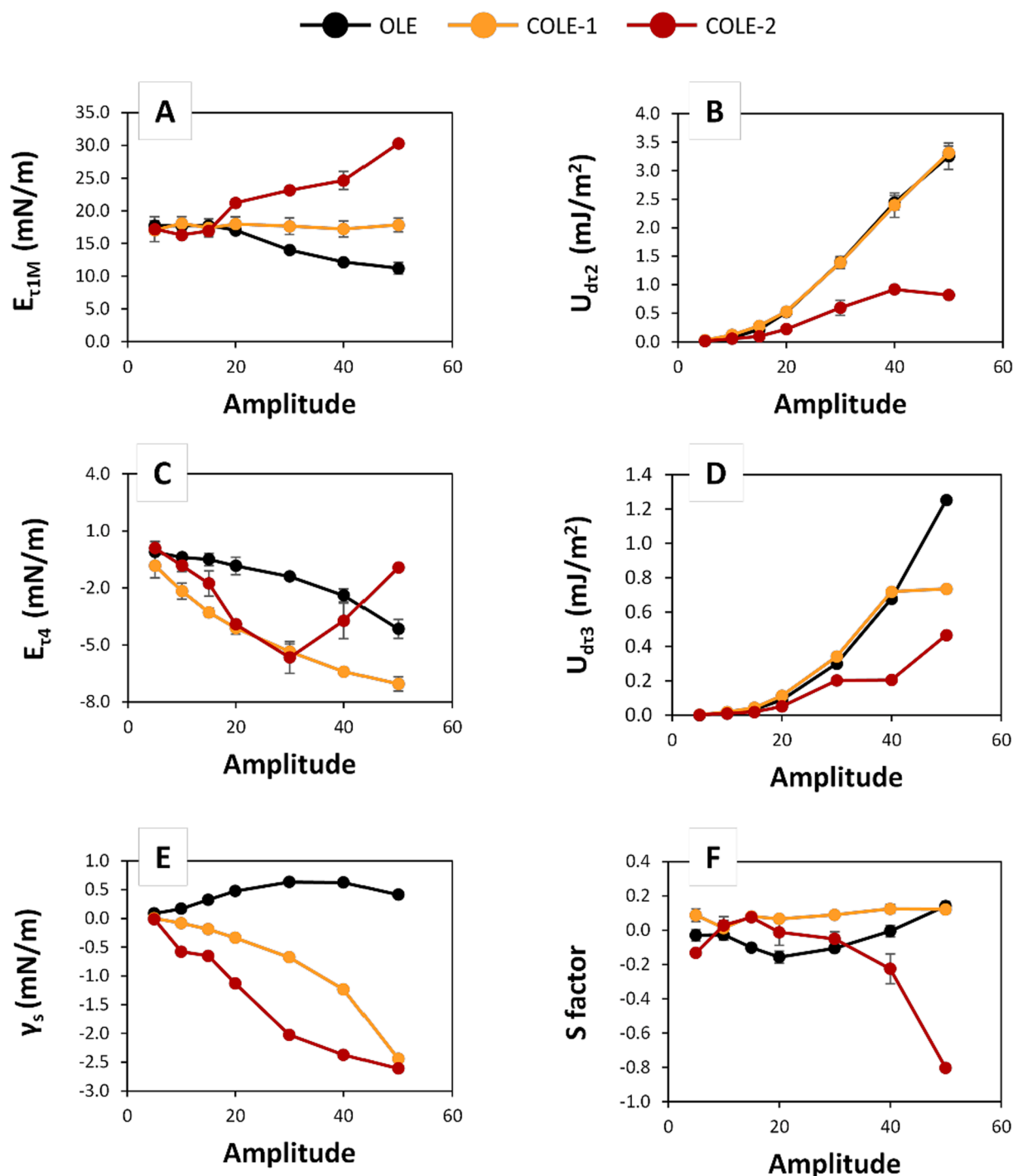


Fig. 4. (A) $E_{\tau1}$; the modulus of $\tau1$, (B) U_{dt2} ; dissipated energy of $\tau2$, (C) $E_{\tau4}$; modulus of $\tau4$, (D) U_{dt3} ; dissipated energy of $\tau3$, (E) γ_s ; vertical shift of $\tau4$, and (F) S factor; strain stiffening factor of $\tau1$ versus deformation amplitude of oleosomes (OLE, black), 0.01 and 0.1 wt% curcumin-loaded oleosomes (COLE-1, orange and COLE-2, red). (For interpretation of the references to colour in this figure legend, the reader is referred to the web version of this article.)

i.e. multilayer formation [33].

Such glassy-like structures could become very dense upon compression, resulting in a significant contribution to the overall stiffness by the changes in surface density ($E_{\tau4}$). This behavior was previously shown for escin-stabilized interfaces at higher deformation, where the interface of escin was so stiff that it led to elongated droplets with a non-Laplacian shape [31]. While the extreme stiffness values observed for escin were not reached by COLE-2, we do see similar behavior, with a flattening off of the response at maximum compression and secondary loop formation, and a corresponding upswing in $E_{\tau4}$ at deformations of

30 % or higher. We did not observe any non-Laplacian shapes of the droplet or buckling, and in view of the complex structure of the oleosome interface (a phospholipid membrane interspersed with much larger oleosins), multilayer formation is unlikely to happen. Therefore, the expulsion of material in compression is most likely the cause of the secondary loop formation in COLE-2. This expulsion could, for example, be by local budding of the phospholipid film [34], followed by retraction of the buds into the interface upon expansion. However, this cannot be confirmed based on rheology data alone.

In summary, curcumin has the ability to increase the interaction

between the oleosome membrane stabilizers. As mentioned in previous work, curcumin is present in the headgroups and the tail of the phospholipids. Here, we show that curcumin can enhance the lateral interactions on the interface, leading to a glassy-like structure, as we saw for the COLE-2 sample. The interface stabilized by COLE-1 has a lower curcumin concentration, and this interface started to partly show the behavior observed for COLE-2. Additionally, the presence of curcumin makes the oleosome (COLE-2) less surface active than the lower curcumin concentration, suggesting a slower rupture on the oil–water interface. These could indicate that COLE-2 has a more rigid membrane that is more stable and slowly rupture.

It has been mentioned that curcumin can affect the stiffness and fluidity of the phospholipid bilayer [35], and the same behavior has been observed for phospholipid monolayers. Other components also increased the attractive interaction (van der Waals forces) between phospholipids, resulting in an increment in surface elasticity [36,37]. For instance, cholesterol and cholesteryl ester behaviors in phospholipid membranes coincide with our hypothesis for curcumin-loaded oleosomes loops. The existence of cholesterol increases the lipid ordering and lipid membrane stiffening in saturated and unsaturated lipid membranes [38,39]. Lipid ordering demonstrates tightly packed membrane lipids, and limited lipids motion [40,41]. Lipid membrane stiffening indicates resistance against deformation, and cholesterol contributes to membrane stiffness by tightly packing lipids [40,42,43].

4. Conclusion

In the present study, we have elucidated the impact of curcumin on the oleosome membrane using interfacial rheology. LAOD and GSD analysis showed that curcumin has the ability to increase the stiffness of the oleosome membrane, indicating that curcumin's presence at the membrane increased the interactions between membrane components (phospholipids and proteins) and the resistance of the oleosome to mechanical deformation. The study provides important insights into the potential applications of oleosomes as carriers and the potential controlled release or targeted delivery of lipophilic cargoes.

CRediT authorship contribution statement

Umay Sevgi Vardar: Writing – original draft, Visualization, Validation, Methodology, Investigation, Funding acquisition, Formal analysis, Data curation, Conceptualization. **Gijs Konings:** Validation, Investigation, Formal analysis. **Jack Yang:** Writing – original draft, Validation, Methodology, Data curation, Conceptualization. **Leonard M.C. Sagis:** Writing – review & editing, Supervision. **Johannes H. Bitter:** Writing – review & editing, Supervision. **Constantinos V. Nikiforidis:** Writing – review & editing, Supervision, Project administration, Funding acquisition.

Declaration of competing interest

The authors declare that they have no known competing financial interests or personal relationships that could have appeared to influence the work reported in this paper.

Data availability

Data will be made available on request.

Acknowledgments

This work was supported by the Ministry of National Education in the Republic of Türkiye.

Appendix A. Supplementary data

Supplementary data to this article can be found online at <https://doi.org/10.1016/j.jcis.2024.09.181>.

References

- [1] S. Bisht, et al., Polymeric nanoparticle-encapsulated curcumin (“nanocurcumin”): a novel strategy for human cancer therapy, *J. Nanobiotechnol.* 5 (2007) 3.
- [2] M. Hasan, et al., Liposome encapsulation of curcumin: physico-chemical characterizations and effects on MCF7 cancer cell proliferation, *Int. J. Pharm.* 461 (1–2) (2014) 519–528.
- [3] T.M. Allen, P.R. Cullis, Drug delivery systems: entering the mainstream, *Science* 303 (5665) (2004) 1818–1822.
- [4] B. Zheng, et al., Loading natural emulsions with nutraceuticals using the pH-driven method: formation & stability of curcumin-loaded soybean oil bodies, *Food Funct.* 10 (9) (2019) 5473–5484.
- [5] B. Zheng, H. Zhou, D.J. McClements, Nutraceutical-fortified plant-based milk analogs: bioaccessibility of curcumin-loaded almond, cashew, coconut, and oat milks, *LWT* 147 (2021) 111517.
- [6] U.S. Vardar, J.H. Bitter, C.V. Nikiforidis, The mechanism of encapsulating curcumin into oleosomes (Lipid Droplets), *Colloids Surf. B Biointerfaces* 236 (2024) 113819.
- [7] M.A. Welte, A.P. Gould, Lipid droplet functions beyond energy storage, *Biochim. Biophys. Acta Mol. Cell Biol. Lipids* 862 (10 Pt B) (2011) 1260–1272.
- [8] C.V. Nikiforidis, Structure and functions of oleosomes (oil bodies), *Adv. Colloid Interface Sci.* 274 (2019) 102039.
- [9] J. Boucher, et al., Sorption of hydrophobic organic compounds (HOC) in rapeseed oil bodies, *Chemosphere* 70 (8) (2008) 1452–1458.
- [10] A. Araiza-Calahorra, M. Akhtar, A. Sarkar, Recent advances in emulsion-based delivery approaches for curcumin: from encapsulation to bioaccessibility, *Trends Food Sci. Technol.* 71 (2018) 155–169.
- [11] E. Ntone, et al., The emulsifying ability of oleosomes and their interfacial molecules, *Colloids Surf. B Biointerfaces* 229 (2023) 113476.
- [12] J. Yang, et al., Air-water interfacial behaviour of whey protein and rapeseed oleosome mixtures, *J. Colloid Interface Sci.* 602 (2021) 207–221.
- [13] M. Deleu, et al., Interfacial properties of oleosins and phospholipids from rapeseed for the stability of oil bodies in aqueous medium, *Colloids Surf. B: Biointerfaces* 80 (2) (2010) 125–132.
- [14] S. Maurer, et al., The Role of Intact Oleosin for Stabilization and Function of Oleosomes, *J. Phys. Chem. B* 117 (44) (2013) 13872–13883.
- [15] G. Waschatko, et al., Soybean Oleosomes Behavior at the Air-Water Interface, *J. Phys. Chem. B* 116 (35) (2012) 10832–10841.
- [16] J. Yang, et al., Competition of rapeseed proteins and oleosomes for the air-water interface and its effect on the foaming properties of protein-oleosome mixtures, *Food Hydrocoll.* 122 (2022) 107078.
- [17] A. Karewicz, et al., Interaction of curcumin with lipid monolayers and liposomal bilayers, *Colloids Surf. B Biointerfaces* 88 (1) (2011) 231–239.
- [18] Y. Sun, et al., The bound states of amphiphatic drugs in lipid bilayers: study of curcumin, *Biophys. J.* 95 (5) (2008) 2318–2324.
- [19] M.J. Romero-Guzmán, et al., Controlled oleosome extraction to produce a plant-based mayonnaise-like emulsion using solely rapeseed seeds, *LWT* 123 (2020) 109120.
- [20] S. Peng, et al., Enhancement of curcumin bioavailability by encapsulation in sophorolipid-coated nanoparticles: an in vitro and in vivo study, *J. Agric. Food Chem.* 66 (6) (2018) 1488–1497.
- [21] A. de Groot, J. Yang, L.M.C. Sagis, Surface stress decomposition in large amplitude oscillatory interfacial dilatation of complex interfaces, *J. Colloid Interface Sci.* 638 (2023) 569–581.
- [22] Y. Yin, et al., 3D reconstruction of lipid droplets in the seed of brassica napus, *Sci. Rep.* 8 (1) (2018) 6560.
- [23] C.J. Beverung, C.J. Radke, H.W. Blanch, Protein adsorption at the oil/water interface: characterization of adsorption kinetics by dynamic interfacial tension measurements, *Biophys. Chem.* 81 (1) (1999) 59–80.
- [24] J. Liu, et al., Spreading of oil droplets containing surfactants and pesticides on water surface based on the marangoni effect, *Molecules* 26 (5) (2021) 1408.
- [25] A.H. Nour, Emulsion types, stability mechanisms and rheology: a review, *Int. J. Innov. Res. Sci. Stud. (IJIRSS)* 1 (1) (2018).
- [26] R.T. van Gaalen, et al., Marangoni circulation in evaporating droplets in the presence of soluble surfactants, *J. Colloid Interface Sci.* 584 (2021) 622–633.
- [27] D. Karefillakis, A. Jan van der Goot, C.V. Nikiforidis, The behaviour of sunflower oleosomes at the interfaces, *Soft Matter* 15 (23) (2019) 4639–4646.
- [28] E.B.A. Hinderink, et al., Behavior of plant-dairy protein blends at air-water and oil-water interfaces, *Colloids Surf. B Biointerfaces* 192 (2020) 111015.
- [29] R.H. Ewoldt, A.E. Hosoi, G.H. McKinley, New measures for characterizing nonlinear viscoelasticity in large amplitude oscillatory shear, *J. Rheol.* 52 (6) (2008) 1427–1458.
- [30] L.M.C. Sagis, K.N.P. Humblet-Hua, S.E.H.J. van Kempen, Nonlinear stress deformation behavior of interfaces stabilized by food-based ingredients, *J. Phys. Condens. Matter* 26 (46) (2014) 464105.
- [31] J. Yang, et al., Surface dilatational and foaming properties of whey protein and escin mixtures, *Food Hydrocoll.* 144 (2023) 108941.
- [32] A. de Groot, L.M.C. Sagis, J. Yang, White asparagus stem proteins, from waste to interface stabilizer in food foams, *Food Hydrocoll.* 146 (2024).

- [33] L.M.C. Sagis, et al., Dynamic heterogeneity in complex interfaces of soft interface-dominated materials, *Sci. Rep.* 9 (1) (2019) 2938.
- [34] W.R. Schief, et al., Nanoscale topographic instabilities of a phospholipid monolayer, *J. Phys. Chem. B* 104 (31) (2000) 7388–7393.
- [35] R.J. Alsop, A. Dhaliwal, M.C. Rheinstädter, Curcumin protects membranes through a carpet or insertion model depending on hydration, *Langmuir* 33 (34) (2017) 8516–8524.
- [36] A.G. Bykov, et al., Dilational surface elasticity of spread monolayers of pulmonary lipids in a broad range of surface pressure, *Colloids Surf. A: Physicochem. Eng. Aspects* 541 (2018) 137–144.
- [37] S. Bhattacharya, S. Haldar, Interactions between cholesterol and lipids in bilayer membranes. Role of lipid headgroup and hydrocarbon chain–backbone linkage, *Biochim. Biophys. Acta (BBA) – Biomembr.* 1467 (1) (2000) 39–53.
- [38] D. Needham, R.S. Nunn, Elastic deformation and failure of lipid bilayer membranes containing cholesterol, *Biophys. J.* 58 (4) (1990) 997–1009.
- [39] F.T. Doole, et al., Cholesterol stiffening of lipid membranes, *J. Membr. Biol.* 255 (4) (2022) 385–405.
- [40] E. London, How principles of domain formation in model membranes may explain ambiguities concerning lipid raft formation in cells, *Biochim. Biophys. Acta* 1746 (3) (2005) 203–220.
- [41] M.D. Weiner, G.W. Feigenson, Presence and role of midplane cholesterol in lipid bilayers containing registered or antiregistered phase domains, *J. Phys. Chem. B* 122 (34) (2018) 8193–8200.
- [42] R.P. Rand, A.C. Burton, Mechanical properties of the red cell membrane. I. Membrane stiffness and intracellular pressure, *Biophys. J.* 4 (2) (1964) 115–135.
- [43] S. Chakraborty, et al., How cholesterol stiffens unsaturated lipid membranes, *Proc. Natl. Acad. Sci. USA* 117 (36) (2020) 21896–21905.